Title
Two distinct components of the delayed single electron noise in liquid xenon emission detectors

Journal
Journal of Instrumentation, 13(02)

ISSN
1748-0221

Authors
Sorensen, P
Kamdin, K

Publication Date
2018-02-01

DOI
10.1088/1748-0221/13/02/p02032

Peer reviewed

Journal of Instrumentation

Two distinct components of the delayed single electron noise in liquid xenon emission detectors

Published by IOP Publishing for Sissa Medialab

Received: *December 14, 2017*
Revised: *January 16, 2018*
Accepted: *February 9, 2018*
Published: *February 27, 2018*

2018 JINST 13 P02032

Two distinct components of the delayed single electron noise in liquid xenon emission detectors

P. Sorensen[a,1] **and K. Kamdin**[a,b]

[a] *Lawrence Berkeley National Laboratory,*
1 Cyclotron Rd., Berkeley, CA, 94720 U.S.A.
[b] *Department of Physics, University of California Berkeley,*
366 LeConte Hall MC 7300, Berkeley, CA, 94720 U.S.A.

E-mail: pfsorensen@lbl.gov

Abstract: Single electron noise which persists for many milliseconds is known to follow ionizing events in liquid/gas xenon emission detectors. Due to the long timescale, this noise can be mistaken for a genuine signal. Therefore, it is a limiting background to the low-energy threshold of dark matter searches, and could prevent discovery-class searches for MeV scale hidden sector dark matter. A systematic study reveals distinct fast and slow components to the noise. The fast component is compatible with the hypothesis of electrons which were trapped below the liquid surface, and can be reduced by increasing the electric field across the liquid/gas interface. However, the slow component increases linearly with electric field. Hypotheses for the origin of this effect are discussed, and techniques for mitigation are suggested.

Keywords: Dark Matter detectors (WIMPs, axions, etc.); Noble liquid detectors (scintillation, ionization, double-phase); Time projection Chambers (TPC)

ArXiv ePrint: 1711.07025

[1]Corresponding author.

https://doi.org/10.1088/1748-0221/13/02/P02032

Contents

2018 JINST 13 P02032

1 Introduction

Liquid xenon emission detectors [1–3] have proven extremely useful for rare-event search experiments, such as for direct detection of galactic dark matter. They are a variant of the time projection chamber in which ionized electrons are drifted to the liquid-gas interface under the influence of an applied electric field E_l. There, the electrons are extracted and drifted through the gas, where they cause proportional scintillation. This technique can easily provide sensitivity to single electrons [4, 5]. The electron emission from the liquid into the gas has a prompt ($\lesssim 0.1\,\mu$s) component and a delayed ($\gg 1\,\mu$s) component [6]. A widely accepted interpretation is that this delayed component is due to electrons which thermalize at the interface and become trapped [7].

In a search for low-mass dark matter, the XENON10 collaboration identified a single electron background which they referred to as an "electron train", with a time scale at least as long as the putative thermalized component [8]. This background is thought to have been responsible for a significant number of the one, two and three electron signals reported in that analysis. A similar background was observed in ZEPLIN-III [4], there-in referred to as 'spontaneous' single electron signals, due to the lack of apparent time correlation with preceding events. More recently, dedicated studies [9, 10] confirmed that indeed the spontaneous signals are time-correlated, and continue for many miliseconds after the primary event.

There is great interest in mitigating this electron noise. It is a potential irritation in the analysis of dark matter search data from instruments such as LUX [11] or XENON1T [12], where it can complicate the classification of low-energy events. It greatly diminishes the discovery potential of these detectors in low-mass dark matter searches [8, 13], or MeV-scale hidden sector dark matter searches [14–16]. It also would complicate efforts to study neutrino neutral current coherent scattering off atomic nuclei [17]. Even a small ($\sim 10\,$kg) liquid xenon emission detector could have significant dark matter discovery potential [18], should it manage to mitigate the single electron noise.

In this article we report results of R&D towards that end, from a systematic study of electron trains in a small liquid xenon emission detector. The data clearly show two components τ_1 and τ_2 in the delayed electron emission, the faster of which (τ_1) can reasonably be interpreted as the initially un-emitted (thermalized) electrons. However, the slower component (τ_2) is not at all consistent with this interpretation.

2 Experimental details

The test bed used to obtain these results was designed to be similar in form and function to the existing dark matter search instruments mentioned in section 1, and is shown schematically in figure 1. It was configured with a 50 mm diameter wire grid cathode and a planar anode. The anode was constructed from gold-coated copper-clad G10 fiberglass, with etched concentric segmentation. The central segment had a 6 mm diameter, with each of two successive segments increasing in radius by 3 mm each. These three segments were each instrumented with a Cremat CR-150 charge-sensitive preamplifier, with a gain of 1.4 mV/fC. The stainless steel grid wires (California Fine Wire, "ultra finish") had 100 µm diameter, and were strung on stainless steel frames with a 2 mm pitch. The anode and the cathode were located 5 mm apart, with a shield grid 10 mm below the cathode.

Xenon was condensed and filled to about 4 mm above the cathode. An electric field E_l was applied in the z direction by biasing the cathode to a voltage $-V$, and holding the anode at ground. Electrons resulting from ionizing radiation were thus drifted toward the anode, and extracted across the liquid-gas interface. The value of E_l contains a systematic uncertainty of ±0.4 kV/cm due to uncertainty in the liquid xenon level. This relationship is described in the appendix. This uncertainty does not affect the basic results, but should be born in mind when comparing against other measurements.

Aqueous ^{210}Po (as $PoCl_4$) was evaporated on a single ~ 1 mm section of a single wire, in the center of the cathode. The literature does not discuss spontaneous deposition[1] of polonium onto stainless steel [19, 20], however, we found it to be robust against dissolution in liquid xenon. Each disintegration of the parent isotope emits into the liquid xenon either a 5.3 MeV alpha particle, or a ^{206}Pb nuclei with a maximum energy of 103 keV. The source spot size was small enough that alpha particle signals only appeared on the central anode segment. This arrangement was made in order to mitigate any effects of electric field fringing near the edges of the active region. The projected range of the alpha particles in the liquid xenon is 41 µm [21], which means they range out under the influence of an electric field which is non-linear and much larger than the bulk field E_l.

A single Hamamatsu R8778 photomultiplier was installed 15 mm below the cathode grid. The photomultiplier was biased to the recommended maximum −1500 V, resulting in easily recognizable single photoelectron pulses and a gain of 1.9×10^7. Voltage records of ionizing radiation events were digitized at 14 bits with 125 MHz sampling and a 20 MHz low-pass filter, with an event duration of 1 ms. Typical events contained both a primary scintillation pulse (S1) and a secondary, proportional scintillation pulse (S2) caused by extracted electrons. A helium after-pulse, a photomultiplier artifact, was often evident 500 ns after the S1. The magnitude of this after pulsing signal was estimated to be about 10% of the originating signal. The average number of photoelectrons

[1] Refers to an irreversible adsorption process, usually of an aqueous metal cation.

2018 JINST 13 P02032

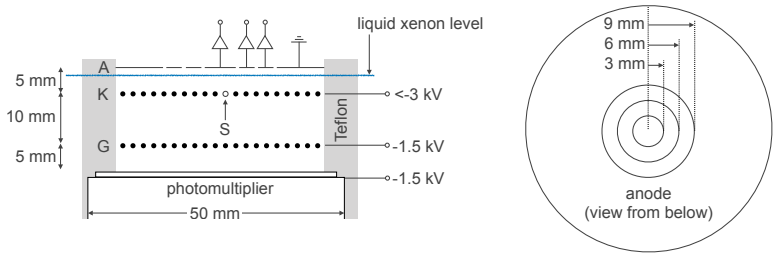

Figure 1. *(Left)* A schematic sectional view of the internal construction of the cylindrical test bed, with segmented anode (A), cathode grid (K), shield grid (G) and the location of the ^{210}Po source (S) indicated. *(Right)* The configuration of the segmented anode as seen from below.

n_{phe} per single electron in the S2 signal was a linear function of the electric field, increasing as $n_{\mathrm{phe}} = 5.77(E_{\mathrm{l}} - 3.25)$, where E_{l} is measured in kV/cm.

Alpha particle S1 consist of $\sim 3 \times 10^5$ scintillation photons [22], of which approximately 10% were collected. This signal easily saturated the anode and the biasing circuit of the photomultiplier [23]. The saturation results in a non-linear response and precludes an accurate measurement of the number of photons present in the S1. The S2 signals consisted of an even larger number of photoelectrons, leading to a complete collapse of the photomultiplier output. This is visible just after 200 µs in figure 2 (middle and bottom). The response recovers in about 30 µs, as expected from the *RC* time of the biasing circuit. The saturation does not adversely affect the experiment, because (a) the alpha particle population was easily identifiable by its size and characteristic drift time (from the cathode), and (b) the number of electrons obtained from alpha particle pulses were measured directly with the charge-sensitive preamplifier.

During operation, the xenon was maintained at a vapor pressure of 1.5 Bar, which implies a fluid temperature of 172 K. Our own temperature measurement recorded 174 K on the outside of the stainless steel vessel which enclosed the xenon. This difference is reasonable considering thermal losses. The xenon was continuously circulated through a heated getter. The liquid was evaporated into a purification loop via a capillary, and the gas was separately purged into the purification loop via a sintered metal filter (to limit the purge rate). The xenon turnover time was about 6 hours, as measured by mass flow. About 2/3 of the flow rate was from the liquid, and the rest from the gas purge. The electron attenuation length was not measured during this experiment, but from comparison with previous experiments and measured charge yields in the literature, can be inferred to have improved to a few tens of cm over the course of a week.

3 Results

Data were acquired at four values of E_{l}, corresponding to $V = [3, 4, 5, 6]$ kV. In each case, the population of ^{210}Po alpha particle events was isolated using simple, robust software cuts on the signal size of S1, S2 and the time delay between them. The waveforms were then stacked (summed) and low-pass filtered. Following this treatment, two distinct exponential components to the delayed electron noise were evident. The decay times of the two components were obtained by fitting a linear function to $y = \log[\Sigma(\alpha \text{ events})]$ over 40 µs (τ_1) and 500 µs (τ_2) regions, indicated by the extent of the fits in figure 2 (bottom). The results are unchanged if this operation is performed on

2018 JINST 13 P02032

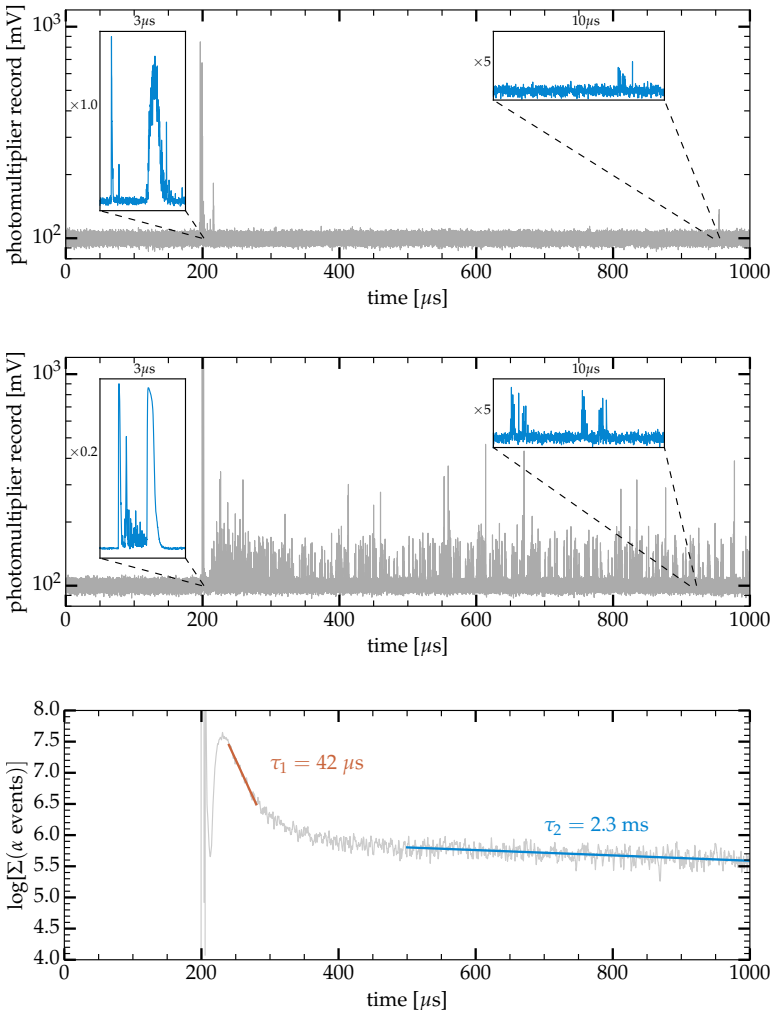

Figure 2. Typical ^{206}Pb recoil and ^{210}Po alpha particle events with $V = 4$ kV, showing inset detail of the primary S1 and S2 structure of the event, as well as a zoom on a portion of the after-pulse region. *(Top)* A ^{206}Pb event record, with $S1 = 130$ detected photons (photoelectrons) and $S2 = 67$ detected electrons. A single electron is visible nearly 800 µs after the primary event. *(Middle)* A ^{210}Po alpha particle event record. *(Bottom)* 400 summed alpha particle event records, low-pass filtered to more clearly illustrate the electron train. Just after 200 µs, the event record shows complete collapse in the photomultiplier response, due to saturation. The recovery time is as expected from the *RC* time constant of the biasing circuit.

either the raw or filtered event records. The τ_1 fit region was chosen to begin 40 µs after the S2, to avoid the region of saturated photomultiplier signal.

The number of delayed single electrons in each component (fast and slow) were obtained by summing the respective portion of the photomultiplier waveform, and dividing by the average single electron size. This procedure was followed because (1) a hand scan of numerous events affirmed that the delayed noise consists overwhelmingly of clearly recognizable single electron pulses, as seen in figure 2 (middle, inset); and (2) often the single electron pulses overlap, so an analysis based on identifying and counting individual electrons would be more likely to suffer from systematic error. Separately, the number of prompt electrons was measured with the charge sensitive preamplifier.

2018 JINST 13 P02032

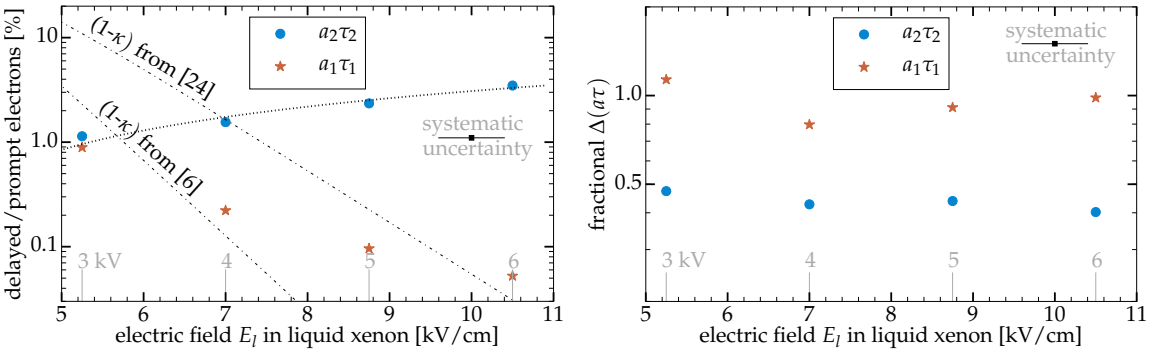

Figure 3. *(Left)* The amplitude of the delayed electron noise is expressed as a percent of the number of prompt electrons in the ionizing event. The fast component $a_1\tau_1$ can be compared against $(1-\kappa)$, where κ is the prompt (occurring in $t \lesssim 0.1\,\mu s$) electron emission efficiency. The slow component $a_2\tau_2$ is fit by a linear function (dotted), whose slope is a factor $\times 13$ smaller than that of the proportional scintillation. *(Right)* The change in amplitude components $a_1\tau_1$ and $a_2\tau_2$ after one week of continuous purification of the liquid xenon. The fast component was not significantly affected by improved liquid purity, while the slow component decreased by a factor $\times 2$. Statistical uncertainty is comparable to the size of the data points.

This ranged from 33, 060 electrons (lowest E_l data point) to 69, 920 electrons (highest E_l data point), and was obtained directly from the prompt ($\sim 1\,\mu s$) step height of the raw charge preamplifier output. Statistical uncertainty on the direct charge measurement was about 8%. The ratio of these numbers is plotted in figure 3 (left), expressed as a percent.

We also observed an increased rate of isolated single photons amongst the delayed electron signal. Some fraction of these photons were due to after-pulsing, the photomultiplier tube artifact described in section 2. Controlling for this and the photomultiplier tube dark counts, delayed single photons seem to be present at a rate of about $\times 0.1$ compared with the number of single electrons. However, because this test bed has no (x, y) resolution in it's scintillation detection, we cannot exclude the possibility that some of these single photons might be due to single electrons whose proportional scintillation yield was very low (such as near the edges of the active region). Therefore, we must consider this as a 10% uncertainty in counting the number of delayed electrons.

The fast (τ_1) and slow (τ_2) components were both assumed to begin at $200\,\mu s$, immediately after the prompt S2, and to extend to infinity. The measured decay time constants of the delayed electron emission were observed to increase with increasing electric field. We found $\tau_1 = \exp(2.62{+}0.157\,E_l)$ and $\tau_2 = \exp(6.32 + 0.214\,E_l)$. The measured amplitudes $a_1\tau_1$ and $a_2\tau_2$ of each component were corrected for the sample measurement window, and are plotted in figure 3 as a percent of the measured number of prompt electrons. The data shown in figures 2 and 3 (left) were acquired after more than a week of continuous purification of the liquid xenon. Figure 3 (right) shows the fractional change in $a\tau$ due to one week of continuous purification. The fast component was not significantly affected by improved liquid purity, while the slow component decreased by a factor $\times 2$.

The fast component of the delayed emission decreases with increasing E_l, suggesting that these are electrons which thermalized at the interface and thus were not emitted promptly. This interpretation can therefore be compared against $(1-\kappa)$, where κ is the prompt (occurring in a time $t \lesssim 0.1\,\mu s$) electron emission efficiency. This comparison tacitly assumes that all electrons which are not emitted promptly are eventually emitted as delayed electrons — an assumption which is certainly challenged by electron capture on electronegative impurities. The function

2018 JINST 13 P02032

$\kappa = [1 + \exp(p_1(-E_l + p_2))]^{-1}$ was used as a parameterization to fit the data from [6, 24]. Ref. [6] is an absolute measurement of the prompt electron emission efficiency, obtained from a charge-sensitive preamplifier. In this case, we found $p_1 = 1.67$ and $p_2 = 3.00$. In contrast, ref. [24] is a relative measurement, obtained from the S2 signal of extracted electrons. It was normalized by assuming the prompt emission reached unity at $E_l = 7\,\mathrm{kV/cm}$. In this case, we found $p_1 = 1.14$ and $p_2 = 3.41$.

The slow component of the delayed electron emission increases linearly with increasing E_l, at a rate which is a factor $\times 13$ smaller than that of the proportional scintillation. This suggests that the physical origin of the effect may be due to the number of proportional scintillation photons, or due to the increase in electric field. A distinct reduction in the magnitude of the slow component is obtained by purifying the xenon, as shown in figure 3 (right).

4 Discussion of the origin of the slow component

The observations suggest that the physical origin of the slow component is electron release from negative ion impurities. If we accept this hypothesis, then it remains to understand what is causing the release of these electrons, and which electronegative impurities contribute most strongly. The dominant mechanisms of electron release from negative ions are photoionization, and direct electron detachment (either via a collisional or a tunneling process). Oxygen is a well-known and unavoidable electronegative impurity in this class of detectors, so it will be considered as an example in the following discussion.

Collisional electron detachment can be expected to have a timescale $t \approx \tau_c/\exp(-E_b/kT)$. Taking $\tau_c = 10^{-13}$ seconds as a typical collision time in the condensed state, and considering the binding energy $E_b = 0.45\,\mathrm{eV}$ of an excess electron to the oxygen molecule, one finds $t \approx 10$ seconds. This should not tend to increase significantly with increasing E_l. On the other hand, the timescale for tunneling would likely decrease with E_l, in contrast with our observation.

Electron detachment due to photoionization could occur if some detector materials were fluorescing, following exposure to the UV photons in the prompt signal. Visible fluorescence would be seen easily by the photomultiplier, at variance with our observation. However, the photomultiplier would be largely blind to infrared fluorescence. Even photons with wavelength in excess of 2.5 μm would have enough energy to photoionize O_2^-. Teflon samples have been previously seen to fluoresce in the visible region [25, 26]. The fluorescence depends on the conditions of Teflon synthesis, and on the impurity type and concentration. The effect of lower temperature is not known. We cannot exclude the possibility that the Teflon used in our test bed construction fluoresce in the infrared. It is also possible that impurities within the xenon produce fluorescence photons.

Finally, we note that the prompt scintillation in xenon is due to de-excitation of the lowest bound states of the xenon excimer [27]. The xenon excimer also has higher-energy bound states [28], which may be excited by the drifting electrons which cause the proportional scintillation. If any of these higher states had lifetimes of several milliseconds, then they could be a source of delayed photons.

5 Conclusions

Delayed, time-correlated single electron noise — sometimes referred to as "electron train" backgrounds — in liquid xenon emission detectors show two distinct components. The fast component

2018 JINST 13 P02032

decreases with E_l and appears to be due to thermalized electrons which were not emitted in the prompt $S2$ signal. The slow component increases with E_l and is consistent with several hypotheses, as discussed in the preceding section. Additional components may exist amongst the delayed electron pulses. These could possibly be resolved with longer-timescale studies. A test bed capable of imaging the (x, y) location of single electrons might also return additional information. And, other classes of delayed electron backgrounds have been noted [10], which are not studied in the present work.

Previous suggestions for mitigation [29] are relevant primarily to the τ_1 component, and therefore would not be sufficient for informing the design of discovery-class liquid xenon emission detectors for MeV-scale hidden sector dark matter. The present work suggests that regardless of the origin of the τ_2 component, an immediate steps towards mitigation of this background is to improve the xenon purity. A future work will attempt to identify the exact origin of this effect, by (1) removing Teflon from the detector construction, and (2) investigating the specific effect of impurity dopants.

A Electric field directly above the ^{210}Po source

For a fixed distance d between cathode and anode, and a liquid height $h < d$, the electric field applied in the liquid is given by $E_l = \epsilon_g V/(\epsilon_l d + (\epsilon_g - \epsilon_l)h)$, in which $\epsilon_l = 2$ and $\epsilon_g = 1$ are the long-wavelength limit of the dielectric constants of the liquid and gaseous states. As required by continuity the electric field in the gas is $\epsilon_g E_g = \epsilon_l E_l$. Near the cathode grid wires, the electric field increases rapidly in strength. The field profile is analytical [30], but cumbersome to write. Figure 4 shows the field profile in the case $V = 4\,\mathrm{kV}$ applied to the cathode, directly above one of the cathode wires.

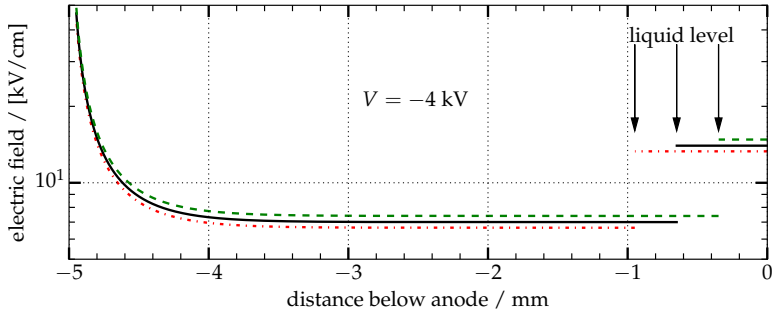

Figure 4. Calculated electric field as a function of liquid level.

There is some width to the distribution of drift times for alpha particles leaving the cathode, and this particular case is useful for comparison against those events with the shortest (cathode-consistent) drift time. The liquid level was estimated from the profile of E_l, along with the measured electron drift time and known electron drift velocity in liquid xenon [31]. Uncertainty in this procedure is estimated to result in a systematic uncertainty of $\pm 0.4\,\mathrm{kV/cm}$, as indicated in the figures.

2018 JINST 13 P02032

Acknowledgments

The authors acknowledge insightful comments from Dan McKinsey and Jingke Xu, and are grateful to the referees for their careful review of the manuscript. This work was supported by the U.S. Department of Energy, Office of Science, Office of High Energy Physics, under award number DE-AC02-05CH1123.

References

[1] A.I. Bolozdynya, V. Egorov, B. Rodionov and V. Miroshnichenko, *Emission detectors*, *IEEE Trans. Nucl. Sci.* **42** (1995) 565.

[2] E. Aprile and T. Doke, *Liquid Xenon Detectors for Particle Physics and Astrophysics*, *Rev. Mod. Phys.* **82** (2010) 2053 [arXiv:0910.4956].

[3] A.I. Bolozdynya, *Emission detectors*, World Scientific, Singapore (2010).

[4] ZEPLIN-III collaboration, E. Santos et al., *Single electron emission in two-phase xenon with application to the detection of coherent neutrino-nucleus scattering*, *JHEP* **12** (2011) 115 [arXiv:1110.3056].

[5] V. Chepel and H. Araujo, *Liquid noble gas detectors for low energy particle physics*, 2013 *JINST* **8** R04001 [arXiv:1207.2292].

[6] E.M. Gushchin, A.A. Kruglov and I.M. Obodovskii, *Emission of "hot" electrons from liquid and solid argon and xenon*, *J. Exp. Theor. Phys.* **55** (1982) 860.

[7] A.I. Bolozdynya, *Two-phase emission detectors and their applications*, *Nucl. Instrum. Meth.* **A 422** (1999) 314.

[8] XENON10 collaboration, J. Angle et al., *A search for light dark matter in XENON10 data*, *Phys. Rev. Lett.* **107** (2011) 051301 [*Erratum ibid.* **110** (2013) 249901] [arXiv:1104.3088].

[9] D.Y. Akimov et al., *Observation of delayed electron emission in a two-phase liquid xenon detector*, 2016 *JINST* **11** C03007.

[10] LUX collaboration, J. Xu et al., *An investigation of the background electron emissions in the LUX detector*, in proceedings of the *APS April Meeting 2016*, Salt Lake City, UT, U.S.A., 16–19 April 2016.

[11] LUX collaboration, D.S. Akerib et al., *Results from a search for dark matter in the complete LUX exposure*, *Phys. Rev. Lett.* **118** (2017) 021303 [arXiv:1608.07648].

[12] XENON collaboration, E. Aprile et al., *First Dark Matter Search Results from the XENON1T Experiment*, *Phys. Rev. Lett.* **119** (2017) 181301 [arXiv:1705.06655].

[13] XENON collaboration, E. Aprile et al., *Low-mass dark matter search using ionization signals in XENON100*, *Phys. Rev.* **D 94** (2016) 092001 [*Erratum ibid.* **95** (2017) 059901] [arXiv:1605.06262].

[14] R. Essig, J. Mardon and T. Volansky, *Direct Detection of Sub-GeV Dark Matter*, *Phys. Rev.* **D 85** (2012) 076007 [arXiv:1108.5383].

[15] R. Essig, A. Manalaysay, J. Mardon, P. Sorensen and T. Volansky, *First Direct Detection Limits on sub-GeV Dark Matter from XENON10*, *Phys. Rev. Lett.* **109** (2012) 021301 [arXiv:1206.2644].

2018 JINST 13 P02032

[16] R. Essig, T. Volansky and T.-T. Yu, *New Constraints and Prospects for sub-GeV Dark Matter Scattering off Electrons in Xenon*, *Phys. Rev.* **D 96** (2017) 043017 [arXiv:1703.00910].

[17] RED collaboration, D.Y. Akimov et al., *Prospects for observation of neutrino-nuclear neutral current coherent scattering with two-phase Xenon emission detector*, 2013 *JINST* **8** P10023 [arXiv:1212.1938].

[18] M. Battaglieri et al., *US Cosmic Visions: New Ideas in Dark Matter 2017: Community Report*, arXiv:1707.04591.

[19] P.E. Figgins, *The Radiochemistry of Polonium*, NAS-NS 3037 (1961) [https://doi.org/10.2172/4034029].

[20] T. Hashimoto, A. Habiro, M. Noguchi and T. Kubota, *Spontaneous deposition behavior of polonium on several kinds of metallic wires and its utilization as a conventional alpha-source*, *Radioisotopes* **39** (1990) 291.

[21] https://physics.nist.gov/PhysRefData/Star/Text/ASTAR.html.

[22] M. Miyajima, S. Sasaki, H. Tawara and E. Shibamura, *Absolute number of scintillation photons in liquid xenon by alpha-particles*, *IEEE Trans. Nucl. Sci.* **39** (1992) 536.

[23] Hamamatsu Photonics K.K. Editorial Committee, *Photomultiplier Tubes: Basics and Applications*, third edition, Hamamatsu Photonics K.K. (2007) https://www.hamamatsu.com/resources/pdf/etd/PMT_handbook_v3aE.pdf.

[24] B.N.V. Edwards et al., *Extraction efficiency of drifting electrons in a two-phase xenon time projection chamber*, 2018 *JINST* **13** P01005 [arXiv:1710.11032].

[25] V.F. Gachkovskii, T.A. Kudryavtseva and N.M. Chirkov, *Dependence of the fluorescence intensity of polytetrafluoroethylene on the conditions of synthesis and molecular weight*, *Bull. Acad. Sci. USSR* **18** (1969) 2297.

[26] S.A. Khatipov et al., *Color and fluorescence of polytetrafluoroethylene treated by γ-irradiation near the melting point*, *Nucl. Instrum. Meth.* **B 269** (2011) 2600.

[27] S. Kubota, M. Hishida and J. Raun, *Evidence for a triplet state of the self-trapped exciton states in liquid argon, krypton and xenon*, *J. Phys.* **C 11** (1978) 2645.

[28] W.C. Ermler, Y.S. Lee, K.S. Pitzer and N.W. Winter, *Ab initio effective core potentials including relativistic effects. II. Potential energy curves for Xe^2, $Xe^+{}_2$, and $Xe^*{}_2$*, *J. Chem. Phys.* **69** (1978) 976.

[29] P. Sorensen, *Electron train backgrounds in liquid xenon dark matter search detectors are indeed due to thermalization and trapping*, arXiv:1702.04805.

[30] W. Blum, W. Riegler and L. Rolandi, *Particle Detection with Drift Chambers*, Springer-Verlag (2008).

[31] E.M. Gushchin, A.A. Kruglov and I.M. Obodovskii, *Electron dynamics in condensed argon and xenon*, *J. Exp. Theor. Phys.* **55** (1982) 650.

2018 JINST 13 P02032